Addressing the surface concentration discontinuity of the core-shell model for lithium iron phosphate batteries

Gabriele Pozzato*, Aki Takahashi*, Xueyan Li†, Donghoon Lee‡,
Johan Ko§, and Simona Onori*,¶

Abstract

This communication addresses the limitation of core-shell enhanced single particle model for lithium iron-phosphate recently published by the authors. In this model, the positive particle surface concentration has a jump discontinuity that forms at the transition from the one-phase to the two-phase region, which is responsible for the positive particle overpotential and open circuit potential jumps seen in the cell output voltage. Such a discontinuity is eliminated by proposing a modification of the core-shell enhanced single particle model based on the bulk-normalized lithium concentration. Simulations results show the effectiveness of the new solution against the previously published one.

1 Introduction

Lithium iron phosphate (LFP) batteries use $LiFePO_4$ as cathode material and are well known for their low resistance properties that enhance their thermal stability and safety, long cycle life and higher current rating. More importantly, in the recent years they have become the lithiun-ion battery technology of choice by major original equipment manufacturers (OEMs) thanks to their cobalt-free design [1].

Three phases are observed: 1) Li-rich phase ($LiFePO_4$), 2) two-phase transition ($LiFePO_4$ and $FePO_4$ are coexisting), and 3) Li-poor phase ($FePO_4$) [2, 3, 4] as a function of the lithium concentration in the positive electrode. A model describing these phase transitions would facilitate the understanding of lithium transport and the effect on electrochemical states, and could be used as a modeling framework for state of charge (SOC) estimators in a battery management system (BMS) design.

Different approaches have been proposed to model phase transitions in LFP batteries [5]. Out of various modeling strategies proposed [6, 7, 8], the core-shell paradigm introduced by [9] is the approach that has gained more attention among battery researchers [10]. In [11] and [12], the authors develop and validate against experimental data a core-shell enhanced single particle model (ESPM) where the transition phases in the cathode – in charge and in discharge – are described

*Energy Resources Engineering, Stanford University, Stanford, CA 94305.

†Assistant manager, Research Team, Tech Center, LG Energy Solution Michigan, Troy, MI 48083

‡Specialist, Data Modeling Algorithm Team, Battery R&D, LG Energy Solution, Daejeon R&D Campus, South Korea 34122

§Professional, Data Modeling Algorithm Team, Battery R&D, LG Energy Solution, Gwacheon R&D Campus, South Korea 13818

¶Corresponding author, sonori@stanford.edu

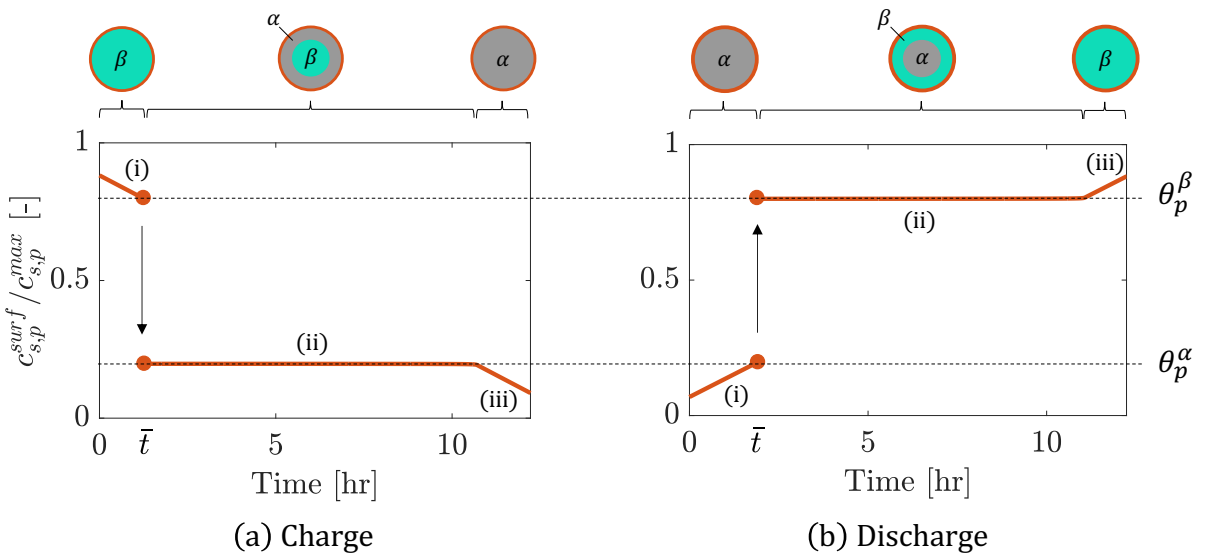

Figure 1: Positive particle normalized surface concentration during charge and discharge. (i) and (iii) indicate the one-phase regions, instead, (ii) is used for the two-phase region. At the one-phase to two-phase transition time instant $\bar{t}$, the surface concentration shows a jump discontinuity from θ_p^β to θ_p^α (charge) or from θ_p^α to θ_p^β (discharge).

by a moving boundary. This model, while effective to reproduce lithiation and delithiation in the positive electrode, produces a discontinuous surface concentration in the positive particle, as shown in Figure 1 for both charge and discharge conditions, where regions (i) and (iii) are the one-phase regions and (ii) is the two-phase transition region. At the transition time instant $\bar{t}$, the normalized surface concentration shows a jump discontinuity and moves from θ_p^β to θ_p^α, during charge, or from θ_p^α to θ_p^β, during discharge. In the core-shell ESPM formulation, the open circuit potentials (OCPs) and overpotentials are a function of the surface concentration [13], hence, this discontinuity affects the positive particle open circuit potential and overpotential calculations which in turns create an artificial jump in the cell output voltage. This limitation of the core-shell modeling paradigm was first observed in [14].

In this work, the discontinuity of the core-shell ESPM is addressed. We propose a modification of the model published in [11, 12] to remove the jump discontinuity during the transition from one-phase to two-phase region (indicated in Figure 1 as (i) and (ii), respectively).

We postulate that the positive particle surface concentration does not transition instantaneously and that using the bulk-normalized concentration would lead to better approximation of the gradual variation in the surface concentration. We refer to the modified core-shell ESPM as the average core-shell model. In the remainder of the paper, equations of the average core-shell ESPM are described, and simulation results are compared with constant current experimental data.

2 Theoretical

In this section, equations for the average core-shell ESPM are introduced. The paper focuses only on the differences with respect to the core-shell ESPM and, for further details on LFP physical principles and governing equations, readers are referred to [12].

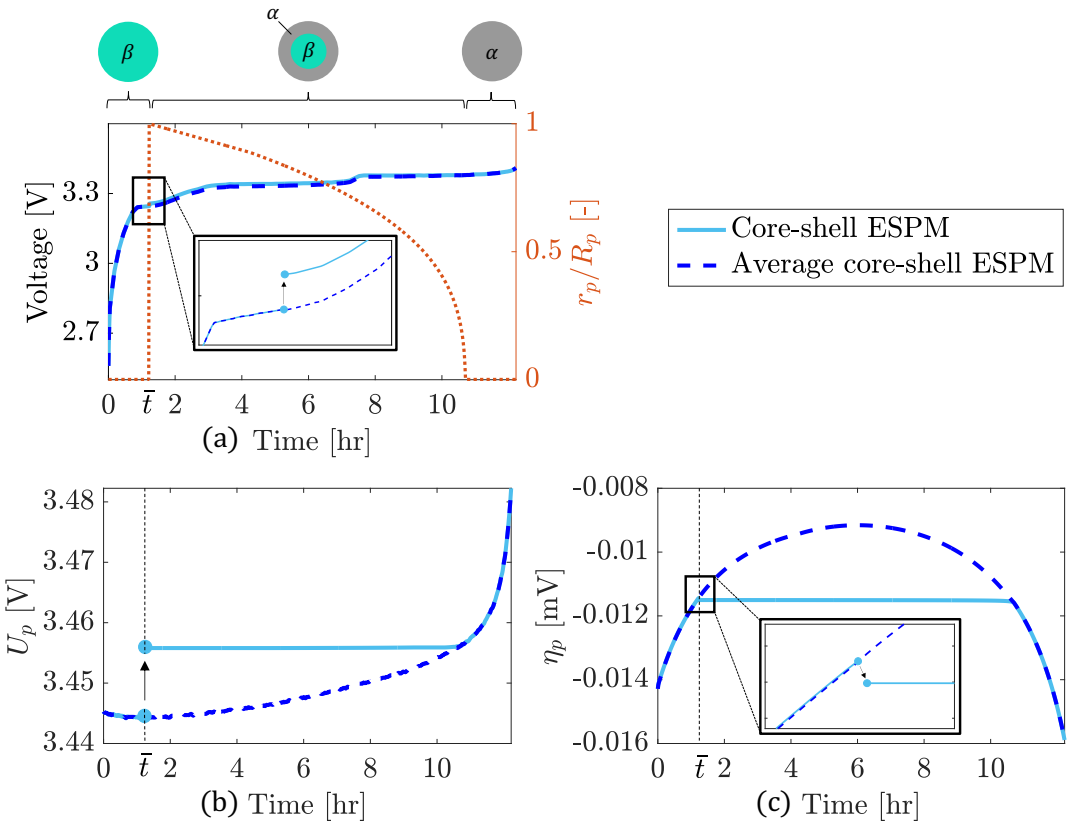

Figure 2: Comparison between core-shell (solid lines) and average core-shell (dashed lines) ESPM considering a C/12 constant current charge simulation. In (a), the simulated output voltage profiles are shown together with the moving boundary r_p, normalized with respect to the particle radius R_p (dotted line). The zoomed portion of (a) shows the 12mV artificial jump present in the core-shell ESPM. The open circuit potential U_p and the overpotential η_p are shown in (b) and (c), respectively. As shown in the plots, the average core-shell ESPM removes the jump discontinuity, leading to smoother profiles in the two-phase region.

2.1 Core-shell ESPM

In the core-shell ESPM, the electrolyte phase is modeled by means of mass and charge transport equations. The positive and negative electrodes (solid phase) are approximated as single spherical particles where lithium intercalation and deintercalation are described by means of mass transport equations. During the $LiFePO_4/FePO_4$ phase transition, two phases are created in the positive electrode: a Li-poor phase (called α) and a Li-rich phase (called β). Both α and β phases are defined in terms of the following normalized lithium concentrations:

$$\theta_p^{\alpha} = c_{s,p}^{\alpha}/c_{s,p}^{max}, \quad \theta_p^{\beta} = c_{s,p}^{\beta}/c_{s,p}^{max} \tag{1}$$

where $c_{s,p}^{\beta}$ and $c_{s,p}^{\alpha}$ are the lithium concentrations for α-phase and β-phase, and $c_{s,p}^{max}$ is the positive particle maximum lithium concentration. The one-phase regions, characterized by one material phase, are formed at the beginning and end of charge and discharge. The positive electrode is in the two-phase region for values of stoichiometry between θ_p^{α} and θ_p^{β} and experiences a phase transition (from β to α, during charge, and from α to β, during discharge). This phase transition is described using the core-shell modeling paradigm, which exploits the moving boundary r_p to model the shrinking phenomena replacing the core-phase with the shell-phase.

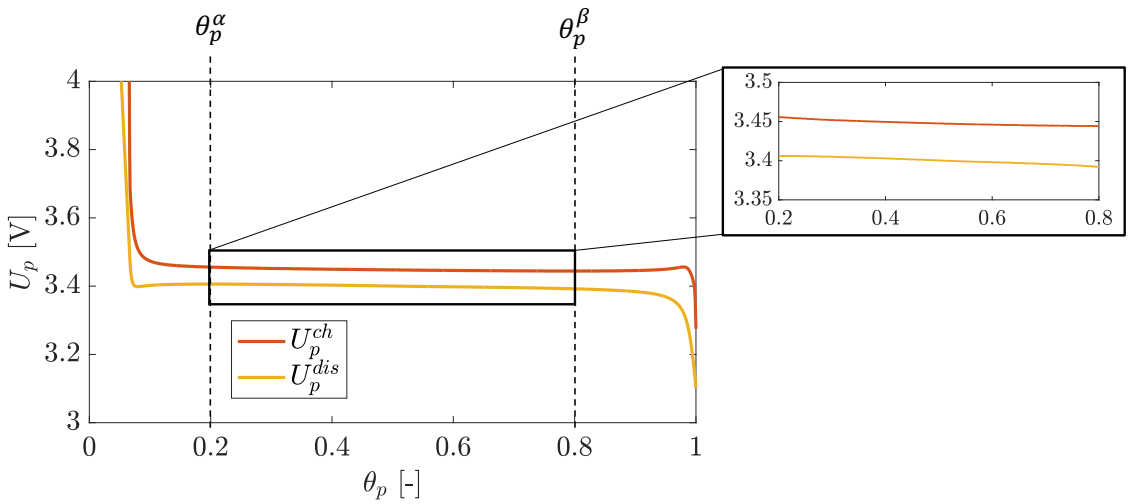

Figure 3: Positive electrode open circuit potentials for charge and discharge. OCPs are collected at C/50 and the zoomed portion of the figure shows the not perfectly constant potential between θ_p^α and θ_p^β.

The bulk-normalized concentration is defined as follows:

$$\theta_p^{bulk} = \frac{3}{c_{s,p}^{max} R_p^3} \int_0^{R_p} c_{s,p} r^2 dr \tag{2}$$

The time at which the one-phase region becomes two-phase is denoted by $\bar{t}$. At this time instant, the bulk-normalized concentration satisfies the following equality:

$$\theta_p^{bulk} = \begin{cases} \theta_p^\alpha, & \text{discharge} \\ \theta_p^\beta, & \text{charge} \end{cases} \tag{3}$$

As shown in Figure 1, at $\bar{t}$, there is a jump discontinuity in the positive particle surface concentration when the transition from θ_p^β to θ_p^α (charge) or from θ_p^α to θ_p^β (discharge) is performed. This discontinuity affects the positive particle kinetic overpotential (η_p) – used to overcome the energy barrier associated with the surface reaction and allow electrons passing through the electrode-electrolyte interface – and open circuit potential (U_p), both a function of the surface concentration [13]. Ultimately, discontinuities in η_p and U_p lead to an artificial jump in the cell output voltage (not present in the experimental data).

Simulation results for the core-shell ESPM during charge are shown in Figure 2 (solid lines), where discontinuities for (a) cell output voltage, (b) U_p, and (c) η_p are highlighted. In our application, a ~12mV jump is observed in the simulated cell output voltage.

2.2 Average core-shell ESPM

As shown in [14], $LiFePO_4$ electrodes are characterized by complex intercalation and deintercalation mechanisms leading to charge and discharge positive particle open circuit potentials which are not perfectly constant in the two-phase region, a behavior observed also in our experimental OCPs in Figure 3. This trait is associated with the non-instantaneous transition of the particle surface concentration from one-phase to two-phase (i.e., from or α to β or β to α), which could be attributed to heterogeneous lithium surface concentrations [4] or the presence of active material particles with a wide size distribution [15].

Table 1: Comparison between core-shell ESPM and average core-shell ESPM.

Core-shell ESPM [12]		**Average core-shell ESPM**	
$\Phi_{s,p} = U_p(\theta_p^{surf}) + \eta_p$	(81)	$\Phi_{s,p} = \begin{cases} U_p(\theta_p^{surf}) + \eta_p, & \text{one-phase} \\ U_p(\theta_p^{bulk}) + \eta_p, & \text{two-phase} \end{cases}$	(4)
$c_{s,p}^{surf} = \theta_p^{surf} c_{s,p}^{max}$	(86)	$\begin{cases} c_{s,p}^{surf} = \theta_p^{surf} c_{s,p}^{max}, & \text{one-phase} \\ c_{s,p}^{bulk} = \theta_p^{bulk} c_{s,p}^{max}, & \text{two-phase} \end{cases}$	(5)
$i_{0,p} = k_p F \sqrt{c^{avg} c_{s,p}^{surf} \left(c_{s,p}^{max} - c_{s,p}^{surf}\right)}$	(88)	$i_{0,p} = \begin{cases} k_p F \sqrt{c^{avg} c_{s,p}^{surf} \left(c_{s,p}^{max} - c_{s,p}^{surf}\right)}, & \text{one-phase} \\ k_p F \sqrt{c^{avg} c_{s,p}^{bulk} \left(c_{s,p}^{max} - c_{s,p}^{bulk}\right)}, & \text{two-phase} \end{cases}$	(6)

To account for this gradual variation in surface concentration, we propose to use the bulk-normalized concentration (calculated through Equation (2)) in place of the surface concentration (as done in [11, 12]) to describe the lithium-ion interaction with the particle surface. This leads to the reformulation of the positive particle open circuit potential U_p and exchange current $i_{0,p}$ shown in Equations (4), (5), and (6). In the one-phase regions, the core-shell ESPM is equivalent to the conventional ESPM [13] and the normalized surface concentration θ_p^{surf} is used to describe the electrode-electrolyte interface. Instead, θ_p^{bulk} is used to model the two-phase region. While the one-phase region does not use the bulk concentration expression, the equality constraint (3) still ensures a smooth transition between one-phase and two-phase.

We refer to this new version of the model as average core-shell ESPM and, as shown in Figure 2(a) and (b) – dashed lines –, it allows to remove the discontinuity present in the output voltage and U_p. Recalling the positive particle overpotential formulation $\eta_p = \frac{RT}{0.5F} \sinh^{-1}\left(\frac{I}{2A_{cell}\ a_p\ L_p\ i_{0,p}}\right)$ and using Equation (6), Figure 2(c) shows the overpotential behavior for the average core-shell ESPM. It is clear that the introduction of the bulk-normalized concentration leads to a a smoother overpotential, removing the nonlinear behavior obtained applying Equations (86) and (88) of [12].

Table 1 compares the equations of core-shell and average core-shell ESPM. For the complete set of equations of the core-shell ESPM and nomenclature, readers are referred to Tables 1, 2, and 3 of [12].

3 Results and Discussion

The model performance is tested over constant current C/12 charge experimental data acquired for a 50Ah pouch cell at 25°C. In [12], experimental data were use to identify the parameter vector:

$$\Theta_{C/12} = \left[R_n, R_p, A_{cell}, D_{s,n}, D_{s,p}, \theta_{n,100\%}, \theta_{n,0\%}, \theta_{p,100\%}, \theta_{p,0\%}, \theta_p^{\alpha}, \theta_p^{\beta}, R_l\right]^T \tag{7}$$

where R_n, R_p, and A_{cell} are geometrical parameters, $D_{s,n}$ and $D_{s,p}$ are solid phase diffusion coefficients that determine the mass transport in the negative and positive particle, $\theta_{n,100\%}$, $\theta_{n,0\%}$, $\theta_{p,100\%}$, and $\theta_{p,0\%}$ define the stoichiometric window of the cell, and R_l is the lumped contact resistance. For the implementation of the core-shell paradigm, θ_p^{α} and θ_p^{β} are also identified.

The identified model parameter vector $\Theta_{C/12}$ is summarized in Table 2. As shown in Figure 4, the model shows a good agreement with the experimental data and no jump is present in the output voltage profile.

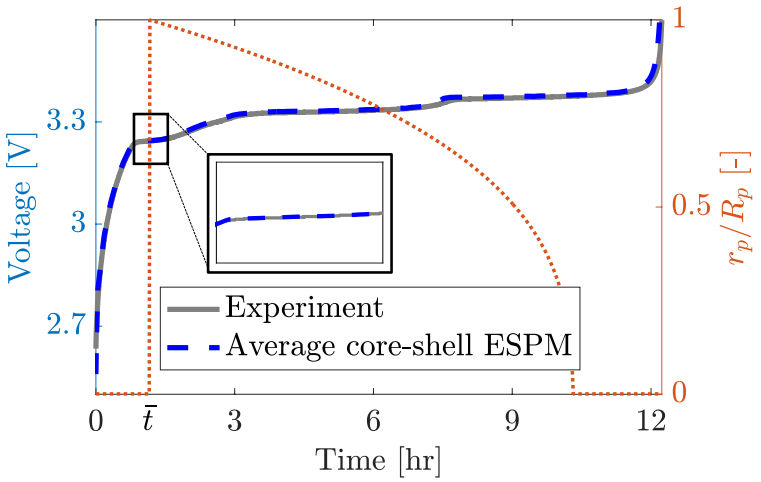

Figure 4: Comparison between simulated and experimental voltage profiles for a C/12 constant current charge at 25°C.

Table 2: Identified model parameter vector $\Theta_{C/12}$ for the C/12 constant current scenario [12].

Parameter	$\Theta_{C/12}$	Unit
R_n	1.03×10^{-6}	[m]
R_p	4.32×10^{-8}	[m]
A_{cell}	1.4910	[m^2]
$D_{s,n}$	6.93×10^{-12}	[m^2/s]
$D_{s,p}$	3.11×10^{-17}	[m^2/s]
$\theta_{n,100\%}$	0.8350	[-]
$\theta_{n,0\%}$	0.0095	[-]
$\theta_{p,100\%}$	0.0696	[-]
$\theta_{p,0\%}$	0.8821	[-]
θ_p^α	0.1980	[-]
θ_p^β	0.8000	[-]
R_l	0.0010	[Ω]

4 Conclusions

This work addressed the limitation of the core-shell model initially proposed by [9] and later developed by the authors. Governing equations are inherited from [12] and, instead of using the surface concentration to calculate U_p and η_p in the two-phase region, the bulk-normalized concentration is introduced. This modification allows to eliminate artificial jumps in the cell voltage when transitioning from one-phase to two-phase region, unlocking the full potential of the core-shell modeling paradigm.

In this framework, the average core-shell ESPM positions itself as a valuable tool for the description of lithium intercalation and deintercalation in $LiFePO_4$ electrodes, and for the design of BMSs. Future improvements of this model include hysteresis and the evaluation of the model performance under real-world operating conditions.

References

[1] A.K. Padhi, K.S. Nanjundaswamy, and J.B. Goodenough, *Journal of the Electrochemical Society*, **144** (4), 1188-1194 (1997).

[2] A. Yamada, H. Koizumi, N. Sonoyama, and R. Kanno, *Electrochemical and Solid State Letters*, **8** (8), A409-A413 (2005).

[3] C. Delmas, M. Maccario, L. Croguennec, F. Le Cras, and F. Weill, *Nature Materials*, **7** (8), 665-671 (2008).

[4] J. Lim, Y. Li, D.H. Alsem, H. So, S.C. Lee, P. Bai, D.A. Cogswell, X.Z. Liu, N. Jin, Y.S. Yu, N.J. Salmon, D.A. Shapiro, M.Z. Bazant, T. Tyliszczak, and W. Chueh, *Science*, **353** (6299), 566-571 (2016).

[5] C.T. Love, A. Korovina, C.J. Patridge, K.E. Swider-Lyons, M.E. Twigg, and D.E. Ramaker, *Journal of the Electrochemical Society*, **160** (5), A3153-A3161 (2013).

[6] W. Dreyer, J. Jamnik, C. Guhlke, R. Huth, J. Moskon, and M. Gaberscek, *Nature Materials*, **9** (5), 448-453 (2010).

[7] C. Delmas, M. Maccario, L. Croguennec, F. Le Cras, and F. Weill, *Nature Materials*, **7**, 665 (2008).

[8] A.S. Andersson and J.O. Thomas, *Journal of Power Sources*, **97**, 498-502 (2001).

[9] V. Srinivasan, and J. Newman, *Journal of the Electrochemical Society*, **151** (10), A1517-A1529 (2004).

[10] S. Koga, L. Camacho-Solorio, and M. Krstic, *Journal of Dynamic Systems Measurement and Control*, **143** (4) (2021).

[11] A. Takahashi, G. Pozzato, A. Allam, V. Azimi, X. Li, D. Lee, J. Ko, and S. Onori. *American Control Conference*, (2022).

[12] G. Pozzato, A. Takahashi, X. Li, D. Lee, J. Ko, and S. Onori, *Journal of the Electrochemical Society*, **169**, 063510 (2022).

[13] E. Prada, D. Di Domenico, Y. Creff, J. Bernard, V. Sauvant-Moynot, and F. Huet, *Journal of the Electrochemical Society*, **159** (9), A1508-A1519 (2012).

[14] M. Safari, M. Farkhondeh, M. Pritzker, M. Fowler, T. Han, and S. Chen, *Electrochimica Acta*, **115**, 352-357 (2014).

[15] K.T. Lee, W.H. Kan, and L. Nazar, *Journal of the American Chemical Society*, **131.17**, 6044-6045 (2009)